

# CuO nanoparticles prepared by alcohol-assisted hydrothermal synthesis for gas-sensing application: effect of pH value

Nguyen Manh Hung<sup>1,†</sup>, Phung Dinh Hoat<sup>2</sup>, Pham Tien Hung<sup>2</sup>, Nguyen Van Hoang<sup>1</sup>

<sup>1</sup>*Department of Materials Science and Engineering,  
Le Quy Don Technical University, Hanoi 100000, Vietnam*

<sup>2</sup>*Department of Physics, Le Quy Don Technical University, Hanoi 100000, Vietnam*

*E-mail:* <sup>†</sup>hungnm@lqdtu.edu.vn

*Received 22 April 2023*

*Accepted for publication 21 November 2023*

*Published 6 December 2023*

**Abstract.** CuO nanoparticles were synthesized by alcohol-assisted hydrothermal method at various pH values, using sodium hydroxide as a precursor for pH control. The chemical composition, morphological and structural properties of the obtained CuO nanoparticles were investigated by the Raman and energy-dispersive X-ray spectroscopies, the field-emission scanning electron microscopy, and the X-ray diffraction. The results reveal that although the pH value does not affect the formation of the CuO phase, it strongly influences the crystalline size, the morphology, and the particle-agglomeration level of CuO. The differences in the morphology and the crystalline size of CuO nanoparticles are ascribed to various H<sup>+</sup>/OH<sup>-</sup> ratios of the growth solution. Meanwhile, with the optimized particle size, the CuO nanoparticles-based sensor can be used as a potential candidate for CO and/or H<sub>2</sub> detection.

**Keywords:** alcohol-assisted hydrothermal; agglomeration; CuO; pH control; H<sub>2</sub> detection.

**Classification numbers:** 65.80.-g; 82.60.Qr.

## 1. Introduction

Cupric oxide (CuO) nanoparticles have attracted a lot of interest from scientists around the world due to their special properties. It is well-known that CuO nanoparticles could be widely utilized for different applications, including magnetic recording [1], photoelectrochemical water splitting [2], energy conversion [3], catalyst [4], and gas sensors [5]. In these applications, CuO

nanoparticles exhibit outstanding characteristics in a comparison to their bulk counterparts. The main factor that leads to such differences is that CuO nanoparticles possess extremely small grain sizes allowing them to make unique chemical and physical properties. Among them, large specific surface area, high porosity, strong catalytic activities, and advanced magnetic characteristics are outstanding properties that are usually used for a number of various applications [6–8]. However, these properties strongly depend on the particle size, crystalline size, and morphology of CuO nanoparticles. Therefore, it is expected that these parameters of CuO nanoparticles could be effectively controlled for practical applications.

Until now, many solutions have been proposed for an effective synthesis procedure of CuO nanoparticles, for example, hydrothermal, solvothermal, sol-gel methods, co-precipitation, thermal decomposition, etc. Among them, the thermal decomposition method of copper salts or their hydroxides was used as a simple method to prepare CuO nanoparticles in large amounts [9]. However, one of the key limitations of this method is that it is difficult to adjust the desired morphology and size of CuO nanoparticles. In the meantime, sol-gel and co-precipitation methods require high-skilled workers. As a result, the repeatability of products prepared by these methods has been proven relatively low. On the contrary, the hydrothermal method possesses high reproducibility in comparison to others mentioned above while allowing the synthesis of CuO nanoparticles in large quantities. However, another aspect of hydrothermal CuO synthesis that needs mentioning is that finding the optimal synthesizing conditions of CuO nanoparticles is a complicated and time-consuming process. Many parameters need to be controlled during a hydrothermal process, such as pH, the concentration of the chemical precursors, solvent, and growing temperature. Because of these reasons, a lot of work has been conducted to intend an optimal process for the hydrothermal synthesis of CuO nanoparticles so far and various results have been reported [10–13]. However, the obtained results show that the morphology and size of CuO are widely distributed when the input parameters fluctuate. This thing leads to significant limitations of CuO nanoparticles in practical applications. Therefore, the researches on the influence of the hydrothermal parameters on the morphological and structural properties of CuO nanoparticles are necessary and should be done further. In the meaning of such intent, in this study, we have investigated the effect of pH on the morphological and structural properties of CuO nanoparticles synthesized by the alcohol-assisted hydrothermal method. The CO and H<sub>2</sub> gas-sensing properties of the CuO nanoparticles-based sensor were also considered in detail.

## 2. Experiment

### 2.1. Synthesis of CuO nanoparticles and sensor fabrication

The chemical reagents of copper acetate ( $\text{Cu}(\text{CH}_3\text{COO})_2$ ,  $\geq 98\%$ ) and diethylene glycol (DEG,  $\text{C}_4\text{H}_{10}\text{O}_3$ ,  $\geq 99\%$ ) were purchased from Sigma-Aldrich Co., Ltd (USA). The absolute ethanol solution ( $\text{C}_2\text{H}_5\text{OH}$ , 99.5%) and sodium hydroxide (NaOH,  $\geq 97\%$ ) were supplied by Samchun pure chemical Co., Ltd (Korea). All the chemical reagents were used in the supplied state without further purification. Firstly, 1 g copper acetate was dissolved into 20 ml deionized (DI) water until obtaining a blue and transparent solution. Secondly, diethylene glycol was added to the solution to reach a solution volume of 100 ml. The pH of the solution then was adjusted by the solution of sodium hydroxide (0.5 M) to ensure that the pH of the solution was remained at pH = 8. The resulting solution was transferred into an autoclave with an inner Teflon-lined reactor

chamber, followed by heating at 120°C for 24h. Finally, after the autoclave was cooled to room temperature, the precipitate was collected by a centrifugation machine and annealed at 400°C for 2h in the air to obtain a black CuO powder. The resulting CuO powder was labeled as S1 sample. Similar processes were also conducted to synthesize other CuO nanopowders with various pH values. The labels of all samples were denoted as in Table 1.

**Table 1.** Sample labels of different CuO nanoparticles were synthesized by DI water + DEG at 120°C with various pH values.

pH	8	9	10	12
Sample	S1	S2	S3	S4
<i>All samples were synthesized at 120°C</i>				

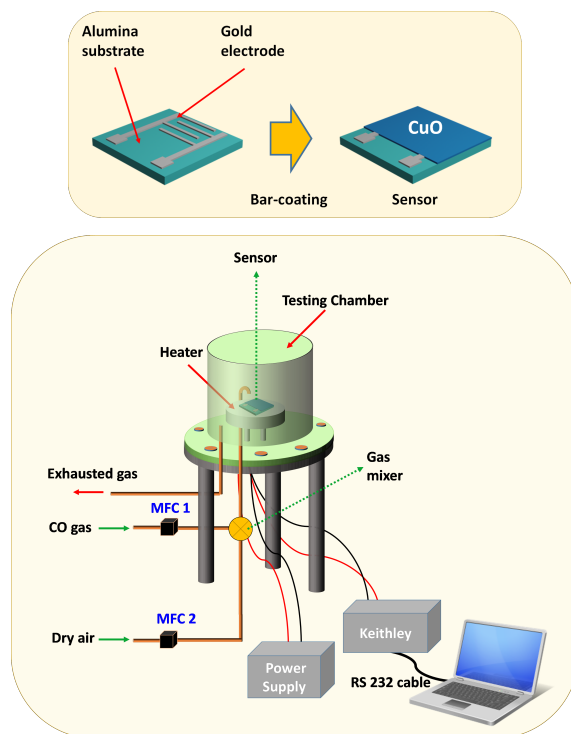


**Fig. 1.** A schematic illustration of the sensor fabrication process and the homemade gas-sensing measurement system.

Alumina substrates patterned with comb-type gold electrodes were utilized to fabricate CuO sensors. The synthesized CuO nanopowder was mixed with a suitable amount of absolute ethanol solution to form a slurry. Then, the slurry was pasted onto the alumina substrate to create a CuO sensor using the bar-coating technique. In order to stabilize the chemical-physical properties for evaluating the gas-sensing performance, the sensor was dried in the air for 30 minutes, followed

by annealing in an air furnace at 500°C for 2 hours. The symbol for the sensor is similar to the label of the material used for the fabrication of its gas-sensing layer. In this work, H<sub>2</sub> and CO gases were chosen as the target gases to evaluate the sensing ability of the fabricated sensor. To create gas mixtures with various CO and H<sub>2</sub> concentrations, CO or H<sub>2</sub> gas flow was diluted by a flow of dry air by controlling the ratio between two flows, using mass flow controllers (MFCs). A homemade gas-sensing measurement system was used for the evaluation of the gas-sensing properties of the sensor as mentioned in our previous works (Fig. 1) [14, 15]. Response (S) of the sensor was determined by  $S = [(R - R_a) / R_a] * 100 \%$ , where R<sub>a</sub> and R are the resistances of the sensor measured in dry air and the gas mixture, respectively. The response time of the sensor is estimated by the time needed for the resistance of the sensor to reach 90% of the saturated resistance value in the gas mixture, while the recovery time is the time that the sensor resistance varied from the saturated value to 90% of base resistance values.

### 2.2. Material characterizations and gas-sensing property measurement

The surface morphology of the synthesized CuO nanoparticles was investigated by the field-emission scanning electron microscopy (FE-SEM, JSM 7610F, JEOL, Japan). The energy dispersive spectroscopy (EDS) integrated with SEM was used to examine the chemical composition of the CuO sample. Structural properties of the CuO samples were analyzed by the X-ray diffraction technique (XRD, X'pert PRO-MPD, PANalytical, Netherlands) and the Raman spectroscopy. The radiation used in the X-ray diffraction measurement is Cu K $\alpha$  radiation ( $\lambda = 0.15418$  nm), while the Raman spectroscopy measurement was conducted at room temperature using an exciting laser source of 532 nm.

## 3. Results and discussion

### 3.1. Structural and morphological characteristics

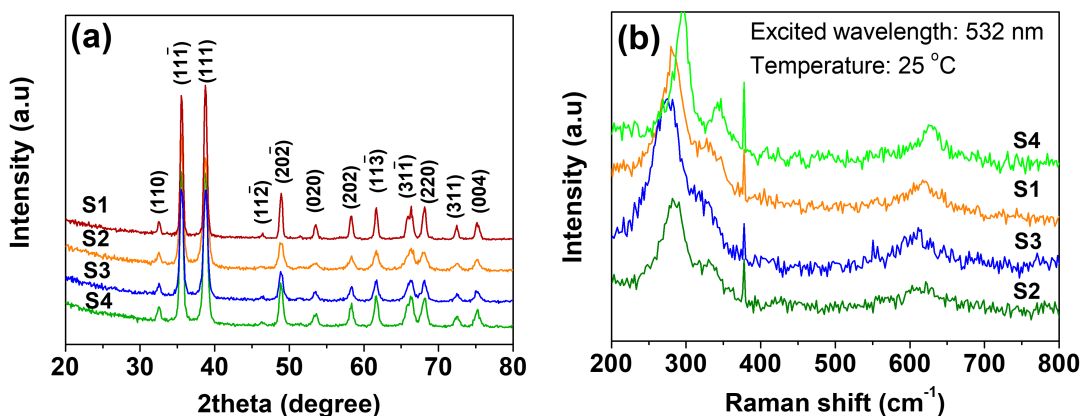


**Fig. 2.** (a) XRD and (b) Raman spectra of CuO samples synthesized by the alcohol-assisted hydrothermal method with various pH values: pH = 8 (S1), pH = 9 (S2), pH = 10 (S3), and pH = 12 (S4).

The X-ray diffraction spectra of all of the fabricated samples display extremely sharp diffraction peaks, indicating the high crystalline quality of all of the samples (Fig. 2(a)). The

peak position and the peak intensity ratio of all the samples are in a good agreement with the monoclinic CuO phase (reference code: 98-008-7123). Moreover, the XRD spectra of all samples are similar. Therefore, it can be assessed that the formation of the CuO phase is not affected by the change in pH value. It is well-known that the Raman spectrum is sensitive to the crystalline state of a solid, particularly crystalline size and crystallinity [16]. Therefore, the Raman spectra of all samples were measured to evaluate the crystalline quality as well as crystalline size, and the results are shown in Fig 2(b). It can be observed that three typical Raman peaks, which are ascribed to various vibration modes, including  $A_g$  ( $280\text{ cm}^{-1}$ ) and  $B_g$  ( $344$  and  $612\text{ cm}^{-1}$ ) of CuO, were observed in all of the samples [16]. In addition, the signal/noise ratio is relatively large for all observed three peaks, suggesting high crystalline quality. These results are consistent with the XRD results mentioned above. J. F. Xu *et al.* have indicated that the Raman peaks of CuO show a slight shift to larger wavenumbers when crystalline size increases [16]. In this study, Raman peaks of S1 and S2 are at similar positions ( $280\text{ cm}^{-1}$ ), while Raman peaks of S3 and S4 samples show shifts. The S3 sample shows a blue shift to a wavenumber of  $278\text{ cm}^{-1}$ . In the meantime, a red shift was observed in  $A_g$  ( $295\text{ cm}^{-1}$ ) peak of the S4 sample. These observations suggest that the crystalline size of the S1 sample should be the smallest and that of the S4 sample should be the largest. Table 2 summarizes FWHM values and corresponding crystalline sizes of synthesized CuO samples were calculated by the Debye-Sheerer formula, indicating a good agreement between the XRD and the Raman spectra. In other words, although the pH value does not affect the formation of the CuO phase, it changes significantly the crystalline size of CuO nanoparticles synthesized by the alcohol-assisted hydrothermal method.

**Table 2.** FWHM values and corresponding crystalline sizes of synthesized CuO samples were calculated by the Debye-Sheerer formula.

Sample	FWHM (degree)	Crystalline size (nm)
S1	0.669	13.7
S2	0.651	14.1
S3	0.726	12.9
S4	0.561	16.4

The morphologies of S1-S4 samples were observed by scanning electron microscopy and shown in Fig. 3. At pH values of 8 and 9, individual CuO nanoparticles and clusters co-exist (Fig. 3(a, b)). There are no significant differences in the morphology of CuO between these two samples. When the pH value reaches 10, the morphology of sample 3 only is consisted of individual CuO nanoparticles without the presence of CuO clusters. The insets in Fig. 3(a, b, c) exhibit that the sizes of CuO nanoparticles in the three samples are similar and approximately 50 nm. At a pH value of 12, CuO strongly changes its morphology, size, and porosity (Fig. 2(d)). The porosity of CuO noticeably decreases, while large nanoparticles along with a wide size distribution (approximately from 50 to 350 nm) are observed. Moreover, some CuO nanorods were also confirmed from the SEM image. Compared to the crystalline size estimated from XRD patterns (Table 2), the particle size is significantly larger than the crystalline size toward each sample. This result suggests that synthesized CuO nanoparticles are polycrystals. During the investigation of the effect of pH value on the morphology of CuO, the synthesizing temperature was remained at

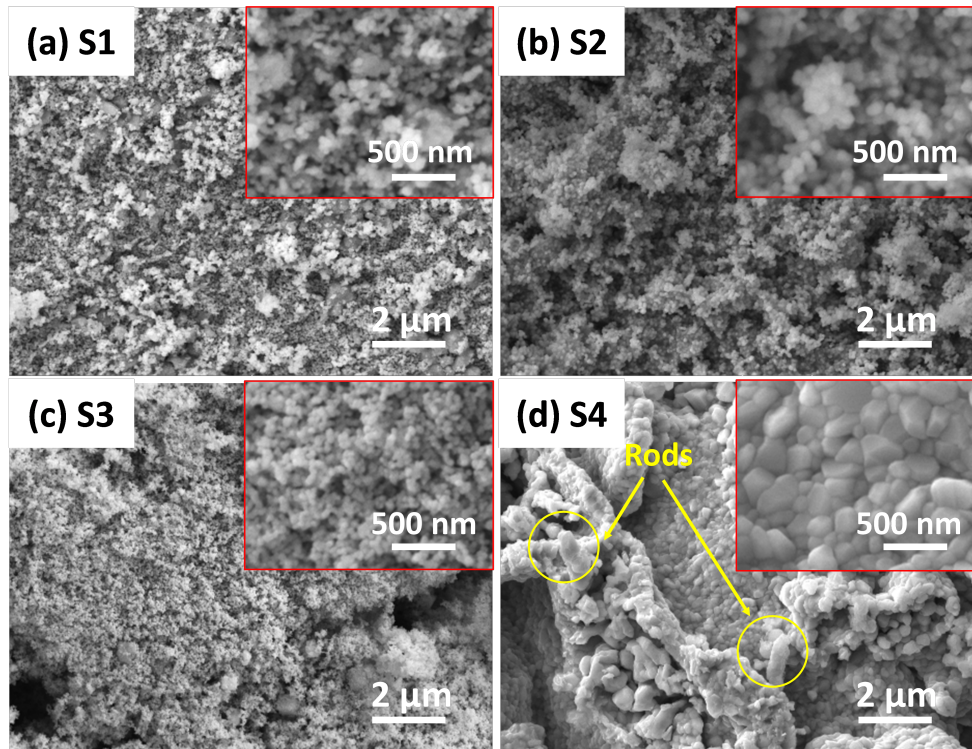
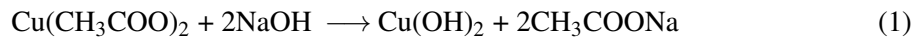


**Fig. 3.** SEM images of CuO nanoparticles synthesized with diethylene glycol solvent at 120°C, and with different pH values: (a) pH = 8; (b) pH = 9; (c) pH = 10; (d) pH = 12. The insets more clearly show the particle size and particle-agglomeration level of the corresponding samples.

120°C, and DEG was used as a growth solvent for all of these samples. Therefore, the effects of the synthesizing temperature and solvent could be removed in considering the mechanism of particle formation. The formation of CuO nanoparticles can be described in the following equations:



Based on equations (1) and (2), the increase of pH value (more NaOH is added to the growth solution) is favorable for the formation of CuO. As a result, the reaction will occur faster at higher pH values. H. F. Abbasov has proposed that the viscosity of polyethylene glycol varies significantly owing to the bound of  $\text{Na}^+$  ions to polymer chains [17]. Therefore, we believe that a similar process also occurs in the DEG solvent and makes the viscosity of DEG increase. Normally, when the viscosity of the solvent decreases, the particle size will become coarser since the atoms are conditioned to diffuse from small particles to large particles. However, in this study, we obtained the opposite result. The coarsening phenomenon becomes more serious when the viscosity of DEG increases owing to the increase of  $\text{Na}^+$  ion concentration (sample S4). Moreover, the appearance of CuO rods in sample S4 suggests that another factor that is not related to viscosity should be a key factor to control the morphology of CuO at a pH value of 12. Chunxia

Li et al. have indicated that the  $\text{OH}^-/\text{H}^+$  ratio is crucial for the growth of the crystal [18]. Clearly, in this study, the  $\text{OH}^-/\text{H}^+$  ratio varies strongly when the amount of NaOH is added to the growth solution. Therefore, the coarse CuO nanoparticles and nanorods that appear in sample S4 could be explained by the strong change in the  $\text{OH}^-/\text{H}^+$  ratio. However, experimental measurements need to be conducted further to confirm the proposed mechanism. Based on the obtained results, we proposed that in order to obtain individual and ultrafine CuO nanoparticles, the pH value of the solvent should be controlled at 10.

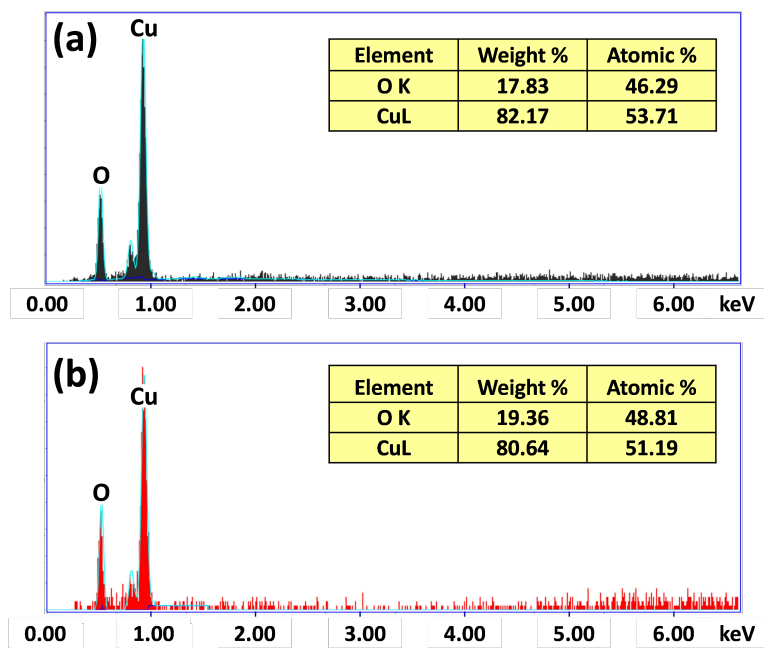


**Fig. 4.** EDS spectra of (a) S3 and (b) S1 samples.

Since the S3 sample reveals the best uniform and ultrafine particle size in comparison to others, the S3 sample was chosen to investigate further by EDS technique and the gas-sensing measurement. EDS result suggests that there are no contaminants in sample S3 under the resolution ability of the EDS equipment (Fig. 4(a)). EDS results also present the atomic percentage of Cu and O atoms are 53.71 and 46.29, respectively. A similar EDS result was also recorded in the S1 sample (Fig. 4(b)). In other words, CuO nanoparticles fabricated by alcohol-assisted hydrothermal are oxygen deficient, which form correspondingly oxygen-vacancy position for the gas-adsorption process on the surface of CuO nanoparticles. This kind of defect is extremely necessary for applications related to surface interactions, such as gas sensors. Therefore, it can be concluded that DEG is an effective solvent for the synthesis of CuO nanoparticles used for gas-sensing applications. Optimal parameters for the synthesis of CuO nanoparticles by DEG solvent, which need to be controlled strictly, include a pH value of 10 and a growth temperature of 120°C.

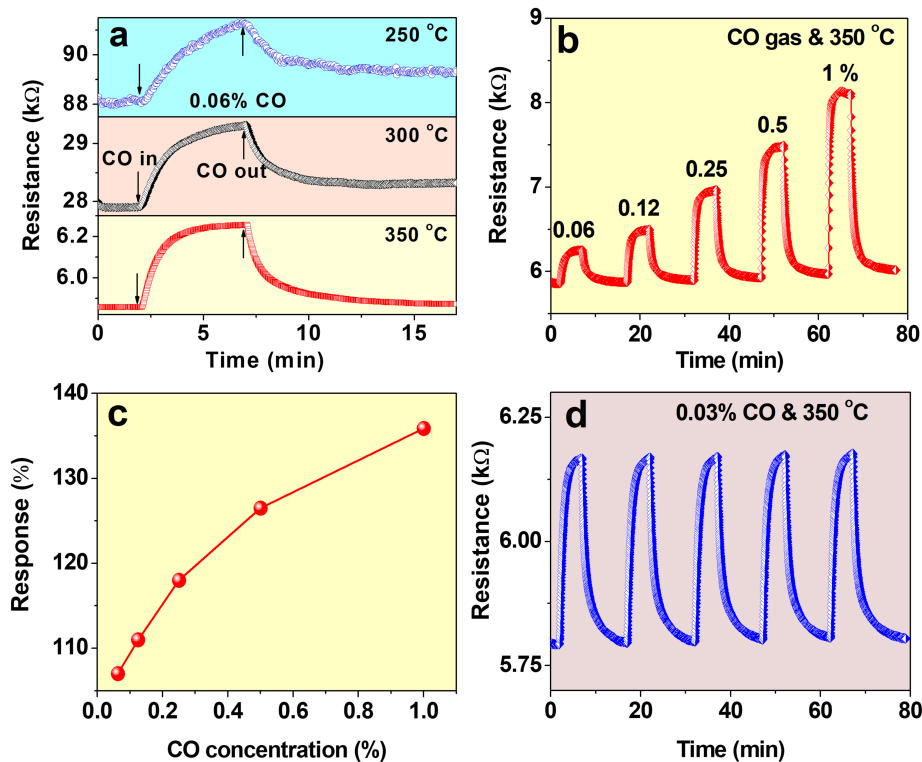


**Fig. 5.** (a) The transient response curves of the CuO nanoparticles-based sensor: (a) toward 600 ppm CO at various temperatures and (b) toward different CO concentrations at 350 °C. (c) A summary of the responses of the sensor derived from (b); (d) The short-term stability of the sensor is evaluated through five response-recovery cycles.

### 3.2. Gas sensing properties and sensing mechanism

Fig. 5(a) shows the change in the resistance of the sensor vs. time when CO gas is supplied to the sensor at three different operating temperatures, including 250 °C, 300 °C, and 350 °C. The sensor exhibits a completely reversible response-recovery cycle at 350 °C, while at lower operating temperatures (250 °C and 300 °C) the recovery process of the sensor is irreversible and/or time-consuming. At 350 °C, the response and recovery times of the sensor are approximately 3 and 5 minutes, respectively. Since the sensor just exhibits reversible response-recovery at 350 °C, we have chosen the operating temperature of 350 °C for the next examinations. Fig. 5(b) displays the changes in the resistance of the sensor toward various CO gas concentrations at 350 °C. Along with a stable resistance base, the sensor exhibits a relatively linear and reversible response-ability for the CO concentration range from 0.06% to 1% (Fig. 6(b, c)). The short-time stability of the sensor is also evaluated by five response-recovery cycles (Fig. 6(d)), which indicates the high repeatability of the sensor. Similar results were also observed for hydrogen sensing shown in Fig. 6 (a, b, c). However, hydrogen shows a slower saturation and recovery compared to CO gas when

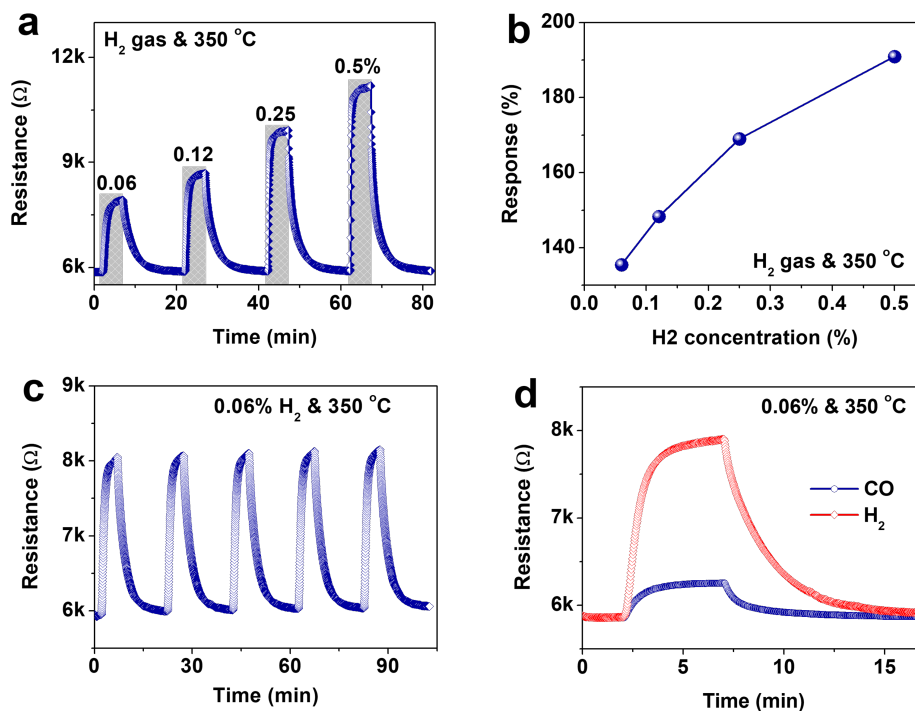


**Fig. 6.** (a) The transient response curve of the CuO nanoparticles-based sensor toward different H<sub>2</sub> gas concentrations at 350°C. (b) A summary of the responses of the sensor derived from (a); (c) The short-term stability of the sensor is evaluated through five response-recovery cycles. (d) The transient response curve of the CuO nanoparticles-based sensor toward CO and H<sub>2</sub> shows a higher response of H<sub>2</sub> gas when both CO and H<sub>2</sub> were examined at similar gas concentrations and operating temperatures.

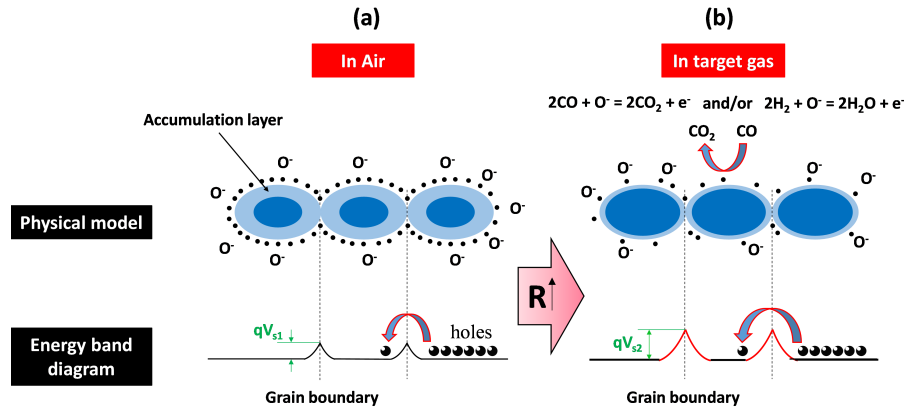
it interacts with the sensor. In contrast, the response level of the sensor toward hydrogen is significantly higher than that of the sensor toward CO gas (Fig. 5(c) and Fig. 6(b, d)). It is worth mentioning that the base resistance of the sensor is relatively stable after each response-recovery cycle. Moreover, the noise signal is extremely small. These factors are favorable for the development of a real gas-sensing device. The CO and H<sub>2</sub> gas-sensing performance of several materials are summarized in Table 3 suggesting the good response level of synthesized CuO nanoparticles-based sensor. However, the response and recovery times of the sensor remain relatively long. Furthermore, we aim to develop a chemo-resistive gas sensor that can selectively detect CO in hydrogen fuel. However, in this study, the hydrogen exhibits a higher response in comparison to the CO gas response. In addition, the operating temperature is relatively high, which can result in a risk of explosion. Therefore, these limitations need to be overcome to reach their real gas-sensing applications.

The resistance of the sensor increases under the presence of CO/H<sub>2</sub> reduced gases suggesting its p-type semiconducting properties of CuO. Therefore, the gas-sensing mechanism of CuO at 350 °C can be illustrated as in Fig. 7. At 350 °C, oxygen atoms attract electrons from the surface

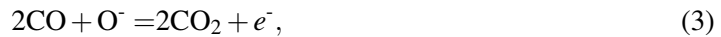
**Table 3.** The gas-sensing performance of synthesized CuO nanoparticles-based sensor compared to other CO and H<sub>2</sub> sensors.

Sensing Material	Target gas	Operating Temperature	Concentration (%)	Response (%)	Ref.
Pt/TiO <sub>2</sub> /MoS <sub>2</sub>	H <sub>2</sub>	100 °C	0.2	74.9	[19]
Pt-TiO <sub>2</sub> /MWCNTs	H <sub>2</sub>	100 °C	5	66	[20]
ZnO film	CO	300°C	0.16	59	[21]
ZnO:Al	CO	400°C	0.1	61.6	[22]
CuO nanowires	CO	300°C	0.01	12	[23]
Y <sub>2</sub> O <sub>3</sub> :ZrO <sub>2</sub>	CO	700 °C	0.04	62	[24]
CuO thin film	CO	300°C	0.5%	15.6	[25]
<b>CuO nanoparticles</b>	<b>CO</b>	<b>350 °C</b>	<b>0.06</b>	<b>106</b>	<b>This study</b>
<b>CuO nanoparticles</b>	<b>H<sub>2</sub></b>	<b>350 °C</b>	<b>0.06</b>	<b>135</b>	<b>This study</b>

All responses (S) were calculated by  $S = [(R_g - R_a)/R_a] * 100\%$  or  $[(R_a - R_g)/R_a] * 100\%$

**Fig. 7.** The illustration of surface reactions and the height of the double Schottky barrier in polycrystalline CuO layers: (a) in air, and (b) under target gases.

layer and exists as ionic species O<sup>-</sup> on the surface of CuO nanoparticles. As a result, a hole accumulation layer is formed at the surface of CuO particles. It should be noted that the conductance of the CuO nanoparticles-based sensing layer is controlled by the thickness of the hole accumulation layer at the surface of the CuO nanoparticles. Because of the adsorption of oxygen atoms, the thickness of the hole-accumulation layer is relatively large. As a result, a double Schottky barrier created at the grain boundary between two adjacent CuO nanoparticles is small (Fig. 7(a)). In the response stage, the presence of CO or H<sub>2</sub> atoms leads to the desorption of ionic species O<sup>-</sup> as shown by the following equations:



The decrease of ionic species  $O^-$  on the surface of CuO nanoparticles results in narrowing the thickness of the hole-accumulation layer, thereby increasing the height of the double Schottky barrier (Fig. 7(b)). The response value of the sensor is proportional to the change in the double Schottky barrier height ( $\Delta qV_b = qV_{s1} - qV_{s2}$ ) as shown in the following equation [26–29]:

$$S = [(R - R_a)/R_a] * 100\% \sim \exp[\Delta qV_b/kT], \quad (5)$$

where  $k$  is the Boltzmann constant and  $T$  is the absolute temperature.

It is worth mentioning that CO and  $H_2$  are gases that are difficult to be detected by chemoresistive gas sensors. Therefore, preliminary gas-sensing results allow us to conclude that CuO nanoparticles synthesized by the alcohol-assisted hydrothermal method in this work can be utilized as an effective gas-sensing material for CO and/or  $H_2$  gas detection if other factors, such as selectivity, and low response are addressed.

#### 4. Conclusions

The effect of pH on the morphological and structural properties of the CuO nanoparticles synthesized by the alcohol-assisted hydrothermal method was investigated. While the pH value does not affect the formation of the CuO phase, it affects significantly the morphology and the crystalline size of CuO nanoparticles. The ratio  $H^+/OH^-$  can be a key reason leading to the differences in the morphology and the crystalline size of CuO nanoparticles. Besides, our preliminary investigations have indicated that the CuO nanoparticles-based sensor has been proven to be a good candidate to detect  $H_2$  and CO gases. However, further studies are necessary to overcome the limitations of this sensor including low selectivity, small response, and high operating temperature.

#### Acknowledgment

This work is financially supported by the Research Support Fund of the Le Quy Don Technical University under Grant Numbers 22.1.18 (3081/QĐ-HV) and 2022.QHT.03 (2942/QĐ-HV).

#### References

- [1] E. Batsaikhan, C.-H. Lee, H. Hsu, C.-M. Wu, J.-C. Peng, M.-H. Ma *et al.*, *Largely enhanced ferromagnetism in bare CuO nanoparticles by a small size effect*, *ACS Omega* **5** (2020) 3849.
- [2] R. Siavash Moakhar, S. M. Hosseini-Hosseinabad, S. Masudy-Panah, A. Seza, M. Jalali, H. Fallah-Arani *et al.*, *Photoelectrochemical water-splitting using CuO-based electrodes for hydrogen production: A review*, *Advanced Materials* **33** (2021) 2007285 [<https://onlinelibrary.wiley.com/doi/pdf/10.1002/adma.202007285>].
- [3] M. Chen, Y. He, Q. Ye, Z. Zhang and Y. Hu, *Solar thermal conversion and thermal energy storage of CuO/paraffin phase change composites*, *International Journal of Heat and Mass Transfer* **130** (2019) 1133.
- [4] A. F. Zedan, A. T. Mohamed, M. S. El-Shall, S. Y. AlQaradawi and A. S. AlJaber, *Tailoring the reducibility and catalytic activity of CuO nanoparticles for low temperature CO oxidation*, *RSC advances* **8** (2018) 19499.
- [5] G. Peng, S. Wu, J. E. Ellis, X. Xu, G. Xu, C. Yu *et al.*, *Single-walled carbon nanotubes templated CuO networks for gas sensing*, *J. Mater. Chem. C* **4** (2016) 6575.
- [6] X. Wang, J. Yang, L. Shi and M. Gao, *Surfactant-free synthesis of CuO with controllable morphologies and enhanced photocatalytic property*, *Nanoscale Res. Lett.* **11** (2016) 1.
- [7] C. Li, S. Chen, X. Gao, W. Zhang and Y. Wang, *Fabrication, characterization and photoelectrochemical properties of cds/cdse nanofilm co-sensitized ZnO nanorod arrays on Zn foil substrate*, *Journal of Colloid and Interface Science* **588** (2021) 269.

- [8] G. Narsinga Rao, Y. D. Yao and J. W. Chen, *Evolution of size, morphology, and magnetic properties of CuO nanoparticles by thermal annealing*, *J. Appl. Phys.* **105** (2009) 093901.
- [9] M. Fukuda and N. Koga, *Kinetics and mechanisms of the thermal decomposition of copper (ii) hydroxide: A consecutive process comprising induction period, surface reaction, and phase boundary-controlled reaction*, *The Journal of Physical Chemistry C* **122** (2018) 12869.
- [10] R. Nithiyavathi, S. John Sundaram, G. Theophil Anand, D. Raj Kumar, A. Dhayal Raj, D. A. Al Farraj *et al.*, *Gum mediated synthesis and characterization of CuO nanoparticles towards infectious disease-causing antimicrobial resistance microbial pathogens*, *Journal of Infection and Public Health* **14** (2021) 1893.
- [11] S. Bilge, B. Dogan-Topal, E. B. Atici, A. Sinağ and S. A. Ozkan, *Rod-like CuO nanoparticles/waste masks carbon modified glassy carbon electrode as a voltammetric nanosensor for the sensitive determination of anti-cancer drug pazopanib in biological and pharmaceutical samples*, *Sensors and Actuators B: Chemical* **343** (2021) 130109.
- [12] L. Zhou, S. Wang, D. Xu and Y. Guo, *Impact of mixing for the production of CuO nanoparticles in supercritical hydrothermal synthesis*, *Industrial & Engineering Chemistry Research* **53** (2014) 481.
- [13] M. Outokesh, M. Hosseinpour, S. Ahmadi, T. Mousavand, S. Sadjadi and W. Soltanian, *Hydrothermal synthesis of CuO nanoparticles: study on effects of operational conditions on yield, purity, and size of the nanoparticles*, *Industrial & engineering chemistry research* **50** (2011) 3540.
- [14] N. M. Hung, N. M. Hieu, N. D. Chinh, T. T. Hien, N. D. Quang, S. Majumder *et al.*, *Rb<sub>2</sub>CO<sub>3</sub>-decorated In<sub>2</sub>O<sub>3</sub> nanoparticles for the room-temperature detection of sub-ppm level NO<sub>2</sub>*, *Sensors and Actuators B: Chemical* **313** (2020) 128001.
- [15] N. M. Hung, N. D. Chinh, T. D. Nguyen, E. T. Kim, G. Choi, C. Kim *et al.*, *Carbon nanotube-metal oxide nanocomposite gas sensing mechanism assessed via NO<sub>2</sub> adsorption on n-wo<sub>3</sub>/p-mwcnt nanocomposites*, *Ceram. Int.* **46** (2020) 29233.
- [16] J. F. Xu, W. Ji, Z. X. Shen, W. S. Li, S. H. Tang, X. R. Ye *et al.*, *Raman spectra of CuO nanocrystals*, *J. Raman Spectrosc.* **30** (1999) 413.
- [17] H. Abbasov, *Effect of sodium hydroxide on the interactions of polyethylene glycol macromolecules with water molecules*, *J. Polym. Res.* **24** (2017) 1.
- [18] C. Li, J. Yang, Z. Quan, P. Yang, D. Kong and J. Lin, *Different microstructures of β-NaYF<sub>4</sub> fabricated by hydrothermal process: effects of pH values and fluoride sources*, *Chem. Mater.* **19** (2007) 4933.
- [19] Y. Luo and C. Zhang, *Pt-activated tio<sub>2</sub>-mos<sub>2</sub> nanocomposites for h<sub>2</sub> detection at low temperature*, *Journal of Alloys and Compounds* **747** (2018) 550.
- [20] L. De Luca, A. Donato, S. Santangelo, G. Faggio, G. Messina, N. Donato *et al.*, *Hydrogen sensing characteristics of Pt/TiO<sub>2</sub>/MWCNTs composites*, *Int. J. Hydrog. Energy* **37** (2012) 1842.
- [21] S. Pati, P. Banerji and S. Majumder, *Mocvd grown ZnO thin film gas sensors: Influence of microstructure*, *Sensors and Actuators A: Physical* **213** (2014) 52.
- [22] J. Chang, H. Kuo, I. Leu and M. Hon, *The effects of thickness and operation temperature on ZnO:al thin film co gas sensor*, *Sensors and Actuators B: Chemical* **84** (2002) 258.
- [23] S. Steinhauer, E. Brunet, T. Maier, G. Mutinati, A. Köck, O. Freudenberg *et al.*, *Gas sensing properties of novel CuO nanowire devices*, *Sensors and Actuators B: Chemical* **187** (2013) 50.
- [24] V. V. Plashnitsa, S. A. Anggraini and N. Miura, *Co sensing characteristics of ysz-based planar sensor using rh-sensing electrode composed of tetrahedral sub-micron particles*, *Electrochem. Commun.* **13** (2011) 444.
- [25] D. Choi, H. Kim, M. Son, H. Kim, H. C. Lee and C. S. Lee, *Fabrication of a kinetically sprayed CuO ultra-thin film to evaluate co gas sensing parameters*, *New J. Chem.* **43** (2019) 7814.
- [26] T. Weis, R. Lipperheide, U. Wille and S. Brehme, *Barrier-controlled carrier transport in microcrystalline semiconducting materials: Description within a unified model*, *J. Appl. Phys.* **92** (2002) 1411 [[https://pubs.aip.org/aip/jap/article-pdf/92/3/1411/10621186/1411\\_1\\_online.pdf](https://pubs.aip.org/aip/jap/article-pdf/92/3/1411/10621186/1411_1_online.pdf)].
- [27] N. V. Hieu, *Textbook of semiconducting metal oxide nanowires-based gas sensors*. Bach Khoa Publishing House, Hanoi, 2015 (in Vietnamese).
- [28] G. Korotcenkov, *Handbook of gas sensor materials: properties, advantages and shortcomings for applications Volume 1: conventional approaches*, vol. 1. Springer, New York, 2013.
- [29] O. Lupan, V. Postica, N. Ababii, M. Hoppe, V. Cretu, I. Tiginyanu *et al.*, *Influence of CuO nanostructures morphology on hydrogen gas sensing performances*, *Microelectronic Engineering* **164** (2016) 63.